Journal of the Korean Electrochemical Society
Vol. 25, No. 1, 2022, 22-31
https://doi.org/10.5229/JKES.2022.25.1.22

Research Paper
pISSN 1229-1935
eISSN 2288-9000

Analysis of Electrochemical Performance of Reduced Graphene Oxide based Symmetric Supercapacitor with different Aqueous Electrolytes

Sneha Ravi, Shivangi Kosta, and Kuldeep Rana*

Electrical Appliances Technology Division, Central Power Research Institute, Bengaluru, India-560080

(Received August 14, 2021 : Revised October 18, 2021 : Accepted October 28, 2021)

Abstract : Carbon nanomaterials are considered to be the materials of choice for the fabrication of electrochemical energy storage devices due to their stability, cost-effectiveness, well-established processing techniques, and superior performance compared to other active materials. In the present work, reduced graphene oxide (rGO) has been synthesized and used for the fabrication of a symmetric supercapacitor. The electrochemical performance of the fabricated supercapacitors with three different aqueous electrolytes namely 0.5 M H_2SO_4, 0.5 M H_3PO_4, and 1.0M Na_2SO_4 have been compared and analyzed. Among the three electrolytes, the highest areal specific capacitance of 14 mF/cm^2 was calculated at a scan rate of 5 mV/s observed with 0.5M H_3PO_4 electrolyte. The results were also confirmed from the charge/discharge results where the supercapacitor with 0.5M H_3PO_4 electrolyte delivered a specific capacitance of 11 mF/cm^2 at a current density of 0.16 mA/cm^2. In order to assess the stability of the supercapacitor with different electrolytes, the cells were subjected to continuous charge/discharge cycling and it was observed that acidic electrolytes showed excellent cyclic stability with no appreciable drop in specific capacitance as compared to the neutral electrolyte.

Keywords : Aqueous Electrolyte, Energy Storage, Reduced graphene oxide (rGO), Supercapacitors

1. Introduction

Supercapacitors (SCs) are one of the fast-evolving electrochemical energy storage devices due to their fast charge/discharge characteristics, high power density, high cycle life, high stability among others. Though they cannot replace batteries completely due to their low energy density; they are being considered for assisting battery-based energy storage systems during high power requirements for short period of time such as in regenerative braking, memory back-up systems and camera flash and as hybrid energy storage solutions for electric vehicles [1,2]. Typical SCs store charge in electrochemical double layers which are formed on the surface of the electrodes and involves no chemical modifications or redox reactions at the electrode material. So, SCs can charge/discharge very quickly and also have longer cycle life, ideally in the order of 100,000 cycles. However, they have limited applications since they possess low energy density compared to other electrochemical energy storage devices such as lithium-ion batteries or fuel cells. In order to enhance the energy density of SCs, various solutions have been considered such as using nano/mesoporous carbon with high specific surface area, use of nanocomposites of carbon with transition metal-oxides [3,4], transition metal-sulphides [5,6], conducting polymers [7,8] among others. The SCs based on such nanocomposites work on the principle of psuedo-capacitance which involves charge storage due to surface redox reactions. Due to this, the power density and cycle life of SCs are compromised since there are surface reactions occurring in these systems which can cause slow degradation of the electrodes as compared to the nano-carbon based SCs. Carbon based materials have researched extensively studied for their use as active materials for SCs due to their numerous advan-

*E-mail: kuldeeprana@cpri.in

tages such as high conductivity, high porosity, large surface area, low cost, and high stability [1,9].

Reduced graphene oxide (rGO) has been studied as an active material for fabrication of SCs. Wang et al. [10] fabricated a reduced graphene oxide membrane based all-solid-state symmetric SC which was synthesized by electrophoretic deposition technique as electrodes and PVA-H_3PO_4 gel electrolyte which showed a high volumetric capacitance, high energy density and high-power density of 107F/cm^3, 7.5 Wh/cm^3 and 2.9 W/cm^3 respectively. Zanin et al. [11] compared the performance of graphene-based films with vertically aligned CNT, both fabricated by chemical vapour deposition technique. Graphene films were prepared using a feedstock of camphor/acetone/citric acid solutions and titanium substrate and the results obtained was similar to those of vertically aligned CNT. 3D Graphene was prepared from graphene oxide, synthesized by one-step hydrothermal treatment was used to fabricate a binder-free SC by Shi and co-workers [12] which exhibited a volumetric capacitance of up to 220 F/g and over 80% capacitance retention under bent state for over 1,00,000 cycles. Trigueiro et al. [13] fabricated a SC based on poly-ionic liquid modified reduced graphene oxide electrodes with ionic liquid 1-methyl-1-propylpyrrolidinium bis (trifluoromethyl sulfonyl) imide as electrolyte which delivered a capacitance of 71.5 F/g with only 10% drop in specific capacitance after 2000 cycles. Sun and co-workers [14] prepared rGO paper using a simple technique of flame induced reduction of graphene oxide paper under room conditions which was used to fabricate SCs with KOH and Et_4NBF_4-acetonitrile solution electrolytes. Both the SCs showed stable cyclic performance with good specific capacitance of 212 F/g and 160 F/g respectively, both calculated at the same current density of 1 A/g.

Apart from these, numerous other works have also been carried out to analyse the performance of graphene oxide [15], graphene [16,17], N-doped graphene electrodes [18], reduced graphene oxide [19,20] and graphene quantum dots [21] as electrodes for symmetric supercapacitors with different electrolytes. The performance of SCs also largely depends on the electrolyte used. Proper combination of electrolyte and electrode materials are crucial for symmetric SCs or electrochemical double layer capacitors (EDLCs) where the charge storage occurs at the electrolyte/ electrode interface. Aqueous electrolytes such as acidic H_2SO_4, H_3PO_4, basic KOH, NaOH or neutral Na_2SO_4 are currently being used in practical SCs since they are environment friendly and their ions can easily penetrate the macro-, micro- or mesopores of carbon-based electrode materials [22]. Apart from aqueous electrolytes, various different electrolytes such as non-aqueous (with and without ionic liquids) [13,23] and solid-state polymer electrolytes [5,10] have also been considered for SC applications. Proper selection of electrolyte with desired characteristics such as ionic conductivity, wide potential window, chemical stability, compatibility with electrode materials and low cost is essential in order to enhance the specific capacitance and energy density of the fabricated SC. Although numerous studies have been carried out on the active materials, limited studies focus on selection of optimal electrolyte and electrolyte concentration for enhancing the performance of the active material when the same is used to fabricate a SC.

In this work, GO was initially prepared using a modified Hummer's method which was reduced using hydrazine hydrate to obtain rGO. Different characterization techniques such as Scanning Electron Microscopy (SEM), X-Ray Diffraction (XRD) and Raman spectroscopy have been used to study the morphology and crystal structure of synthesized material which was further used for fabricating symmetric SCs. A comparative study on the performance of the SC fabricated was carried out with three different aqueous electrolytes (0.5M H_2SO_4, 0.5M H_3PO_4 and 1.0M Na_2SO_4) through electrochemical performance studies such as cyclic voltammetry (CV), galvanostatic charge-discharge (GCD) and electrochemical impedance spectroscopy (EIS). The results obtained were analysed and compared in order to select suitable electrolyte which is most compatible with rGO based electrodes.

2. Experimental

2.1 Synthesis of graphene oxide and reduced graphene oxide

In order to synthesize rGO, graphene oxide (GO) was synthesized from graphite by using a modification of the hummer's method [24,25]. 1 g of Graphite was

added to 9:1 mixture of concentrated H_2SO_4/H_3PO_4. The mixture was kept in ice bath maintained at 0-5°C for 1hr after which 6g of potassium permanganate was added to mixture slowly while maintaining its temperature within 20°C. The mixture was vigorously stirred for one hour after which the ice bath was removed and the temperature of the mixture was raised to 40°C which was maintained for 24 hours. The reaction mixture was cooled to room temperature after which it was poured over ice containing 30% H_2O_2 to obtain a bright yellow suspension. The suspension was washed repeatedly using 3M HCl, ethanol and DI water to remove contaminants after which GO solids were filtered out and dried in vacuum at 80°C.

rGO was prepared from the GO synthesized by reduction using hydrazine hydrate [26]. 0.5 mg of hydrazine hydrate was added to a 500 mL suspension of GO, with GO at a concentration of 3 mg/mL. The mixture was placed in an oil bath at 80°C for 12 hours and stirred continuously. rGO obtained was filtered out and washed using ethanol and DI water multiple times. The obtained rGO solids were dried at 80°C under vacuum.

2.2 Characterization

rGO synthesized was characterized by using SEM, XRD and Raman spectroscopy. The PANalytical X'Pert Pro x-ray diffractometer with a Cu Kα source was used to obtain the XRD spectrum of synthesized material. Carl Zeiss EVO18 Scanning Electron Microscope was used to obtain the high-resolution images of the sample at 15 kV. Raman spectroscopy was performed using Horiba LabRAM Aramis at a laser power of 15mW.

2.3 Fabrication of symmetric supercapacitor (rGO-SC)

The rGO based electrodes for the symmetric SC were prepared by coating the slurry of the solids with PVDF binder onto Nickel foils followed by drying under vacuum at 80°C in order to remove the solvent (NMP) used for the binder. After drying the electrodes, the SC was assembled by placing a cellulose paper between the electrodes as separator and the assembly was sandwiched between two flexible Polyethylene terephthalate (PET) films. The SC was tightly sealed using cellophane in three sides after which the electrolyte was injected by means of a syringe. After injecting the suitable amount of electrolyte, the SC was sealed completely. The schematic representation of the fabrication process is depicted in Fig. 1(a) and photograph of the fabricated symmetric SC is as shown in Fig. 1(b) and Fig. 1(c) respectively. In this work, the performance of rGO based SCs was studied with

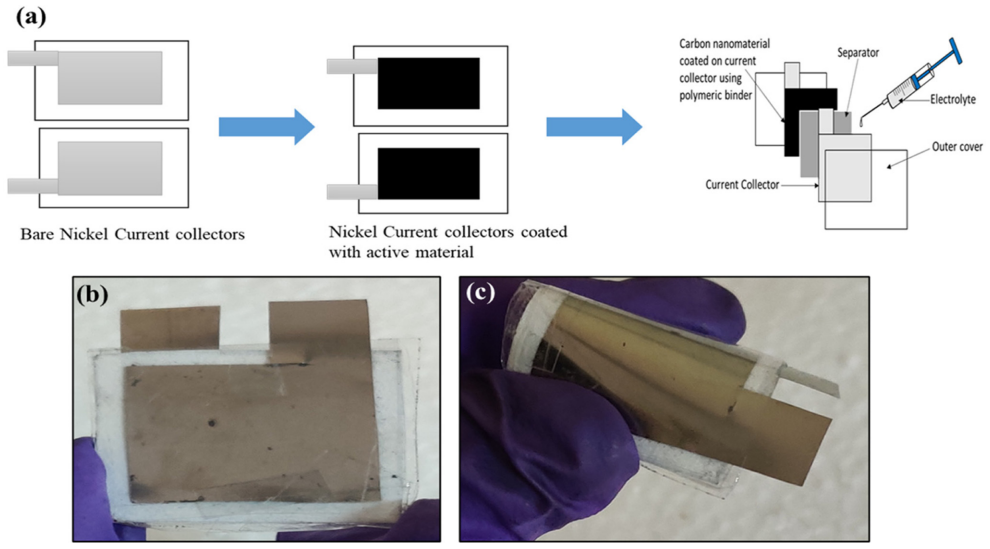

Fig. 1. (a) Schematic representation of fabrication of the symmetric supercapacitor (b-c) Photograph of the fabricated cell

three different aqueous electrolytes namely 0.5 M H_2SO_4, 0.5 M H_3PO_4 and 1.0 M Na_2SO_4 in order to select the electrolyte most compatible with rGO nanomaterials.

2.4 Electrochemical performance of the rGO-SC fabricated with different electrolytes

Various electrochemical techniques such as cyclic voltammetry (CV), Galvanostatic charge/discharge (GCD), Electrochemical Impedance Spectroscopy (EIS) and cyclic stability studies. Ametek PARSTAT MC-1000 multichannel potentiostat was used to carry out these studies. The CV curves for the SCs were obtained in voltage window of –1 V to 1 V at various scan rates ranging from 5 mV/s to 100 mV/s. The EIS studies were performed at the sinusoidal amplitude of 10 mV with the readings taken over a frequency range from 1 MHz to 10 mHz. The GCD studies were carried out for the SCs in the voltage window of 0 V to1 V at current densities varying from 0.08 mA/cm^2 to 2 mA/cm^2.

3. Results and Discussion

The morphology of the synthesized nanomaterial was analysed using SEM imaging. As observed in Fig. 2(a) before reduction process, we observe a layered structure which confirms the successful exfoliation of graphite to graphene oxide (GO). The SEM images for rGO obtained at two different magnifications are shown in Fig. 2(b). It can be observed that the synthesized rGO material has flake-like layered structure with visible pores and cracks generated during reduction process of graphene oxide (GO). The crystal structure and phase characteristics of the synthesized material after reduction of GO was studied using XRD and the pattern obtained is illustrated in Fig 2(c). The wide peak obtained at around 27° and at 44° can be indexed to [002] and [102] plane of hexagonal-graphitic layers. The wide peak obtained at 27° indicates slightly amorphous and disordered nature of the synthesized material. XRD pattern confirmed the successful elimination of oxygen functional group from GO. The wide spread of the peaks in XRD pattern indicate the large interlayer spacing.

Raman spectrum of the synthesized rGO is demonstrated in Fig 2(d) which shows two well-known peaks (D & G band) of first order Raman spectrum at 1330 cm^{-1} and 1570 cm^{-1} respectively for graphite. The D-band corresponds to the presence of defects and disorder in structure whereas

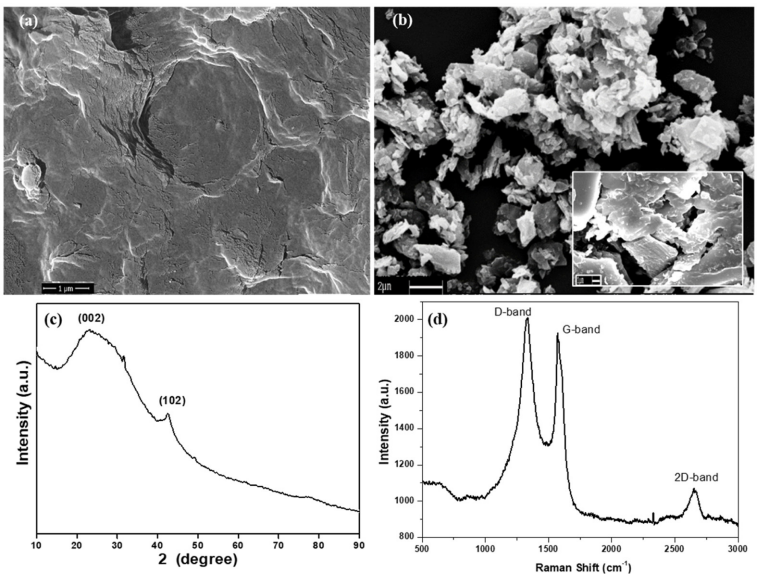

Fig. 2. SEM Images of (a) GO and (b) rGO at low and high magnification (inset) (c) XRD spectra and (d) Raman spectra of synthesised rGO material

G- band corresponds to in plane vibration of sp^2 carbon atoms. The second order peak (2D) of D-band has also been observed at around 2650 cm^{-1}. The intensity ratio (I_D/I_G) calculated around 1.04 indicates there are high defect levels due to edge surface defects and vacancies in the carbon structure, which improves the electrochemical performance of the cell [19]. In order to understand the electrochemical performance of rGO based electrodes, three different SCs have been fabricated and studied using three different electrolytes (acidic H_3PO_4, H_2SO_4 and neutral electrolyte Na_2SO_4). The electrochemical performances such as CV, GCD and EIS spectra have been evaluated, analysed and compared the results obtained and discussed in detail.

Electrochemical measurements of the fabricated supercapacitor were performed at ambient conditions using different electrolyte was first studied using CV performed at scan rates varying from 5 to 100 mV/s. Fig. 3(a-c) shows the cyclic voltammetry curves obtained for three different SCs fabricated with different electrolytes taken at wide range of scan rates ranging from 5 mV/s to 100 mV/s. The areal capacitance (C_{sp}) of the SC can be calculated from the CV curves using the following formula:

$$C_{sp} = \int \frac{idV}{2 \times \Delta V \times \nu \times A} \quad (1)$$

where, $\int idV$ is the area under the CV curve, ΔV is the voltage range (V), ν is the scan rate (V/s) and A is the surface area of the electrodes [2,27].

The CV curves obtained from the SCs with three different electrolytes are as demonstrated in Fig. 3(a-c), the specific capacitance of the cells calculated using the formula (1) are compared in Fig 3(d). The near rectangular shape of the CV curves indicates EDLC behaviour. The SC with H_3PO_4 electrolyte demonstrates the highest specific capacitance of 14 mF/cm^2 calculated at a scan rate of 5 mV/s and 7 mF/cm^2 at a scan rate of 100 mV/s. The cell with H_2SO_4 electrolyte shows similar specific capacitance of 14 mF/cm^2 at 5 mV/s however decreases at high scan rates with a calculated spe-

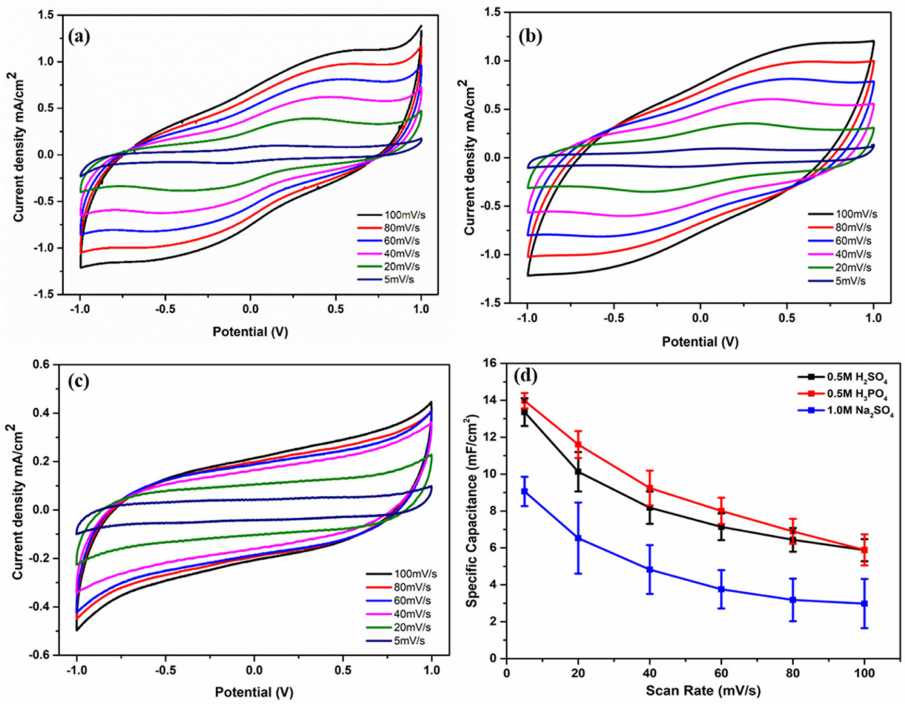

Fig. 3. (a-c) CV curves at different scan rates for cells with H_2SO_4, H_3PO_4 and Na_2SO_4 electrolytes respectively (d) Variation of areal specific capacitance with scan rates for cells with H_2SO_4, H_3PO_4 and Na_2SO_4 electrolytes

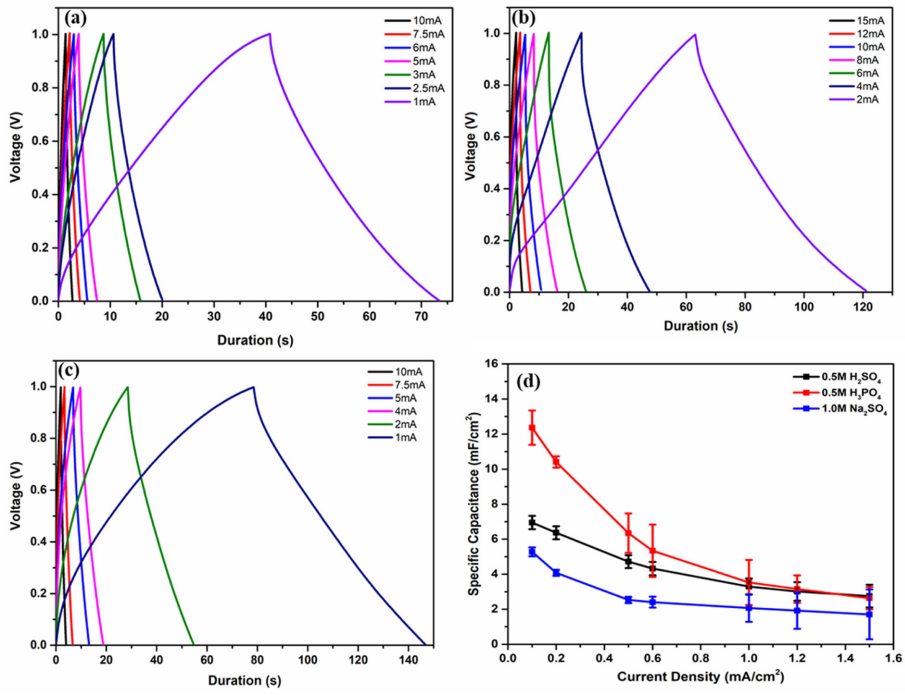

Fig. 4. (a-c). CD curves at different scan rates for cells with H_2SO_4, H_3PO4 and Na_2SO_4 electrolytes respectively (d) Variation of areal specific capacitance with discharge current for cells with H_2SO_4, H_3PO_4 and Na_2SO_4 electrolytes

cific capacitance of 6 mF/cm^2 at 100 mV/s. The variation of specific capacitance of the SCs with different electrolytes can be attributed to the difference in the diffusion rates of the hydrated ions or ionic conductivity of the electrolyte. Higher ionic conductivity and comparable size of ions and electrode surface delivers enhances the specific capacitance of the cell. As previously reported in literature, the ionic conductivity of different cations is in the order of $H^+ > Na^+$ while the values for the cations is in the order $PO_4^{3-} > SO_4^{2-}$ [28,29] which is in agreement with the results obtained for the three electrolytes. Also, at low scan rates, most of the surface of the rGO material is accessible to the electrolyte ions leading to higher specific capacitance values. The cells with acidic electrolytes show moderate decrease in specific capacitance even at high scan rates which implies that the surface of rGO is accessible to electrolyte ions even at high scan rates.

The performance of the cell was also been studied by GCD studies at various current densities. The behaviour different SCs with the three electrolytes can been seen in Fig. 4(a-c), respectively. The GCD profiles were used to calculate the specific capacitance (C_{sp}) of the symmetric SCs using the formula:

$$C_{sp} = \frac{I \times \Delta t}{A \times \Delta V} \quad (2)$$

where, I denotes the discharge current (A), A denotes the geometric surface area of the electrode (cm^2) and $\frac{\Delta V}{\Delta t}$ is obtained from the slope of the discharge curve (V/s) [16,30].

The GCD curves for all the electrolytes are triangular which indicates purely EDLC behaviour of charge storage. The SC fabricated with H_3PO_4 electrolyte demonstrated the highest specific capacitance of 11 mF/cm^2 at a current density of 0.16 mA/cm^2. The values of specific capacitance obtained from charge-discharge profiles are consistent with the values of specific capacitance obtained using cyclic voltammetry data. IR drop can be observed with all the three electrolytes which can be attributed to the

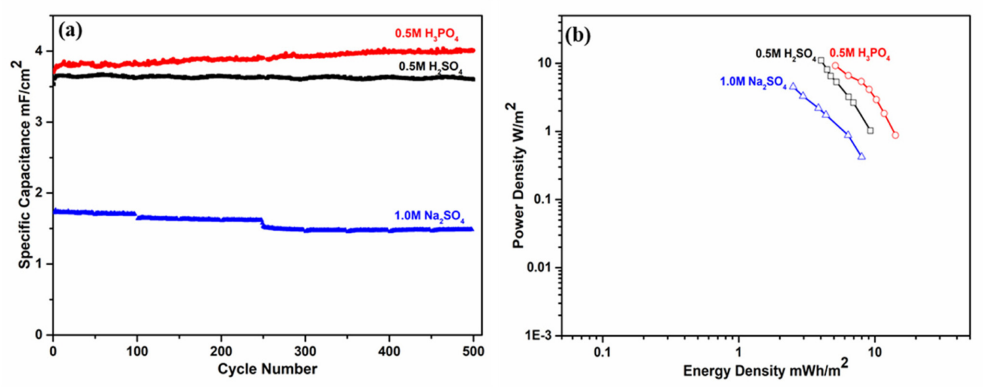

Fig. 5. (a) Specific capacitance calculated at a current of 1 mA/cm^2 during continuous cycling for 500 cycles (b) Ragone plot for cells with H_2SO_4, H_3PO4 and Na_2SO_4

resistance offered by the electrolyte to ion diffusion to the interior structure of the electrodes [28].

In order to assess the long-term performance of the SCs, it was subjected to continuous charge and discharge cycling. The life cycle test has been conducted on all three SCs and variation of specific capacitance with cycle number are shown in Fig. 5 (a). The cells with acidic electrolyte showed excellent cyclic stability up to 500 cycles with no significant drop in the specific capacitance even after 500 cycles. However, the cell with neutral electrolyte showed slight degradation in capacitance with cycling and had a capacitance retention of 86 % after 500 cycles. The degradation in neutral electrolyte can be attributed to the formation of oxygenated functional groups on the electrode surface which leads to decrease in the specific capacitance of the cell and lower ionic conductivity when compared to the other electrolytes [28,31]. The energy density and power density of the cells was calculated using previously reported methods [32] and the obtained values are shown in Fig. 5 (b). From the Ragone plots for the cells, it is observed that the SC with H_2SO_4 electrolyte delivers the highest power density of 11 W/m^2 measured at a current density of 2 mA/cm^2.

The variation in the values of specific capacitance, energy density and power density of the rGO based SC with different electrolytes can also be attributed to its equivalent series resistance (ESR). The ESR gives a combined resistance which includes ionic resistance of the electrolyte, intrinsic resistance offered by the active material, the contact resistance between the active material and the current collector and the resistance offered by the electrical contacts [16,22]. Low values of ESR with phase angle of EIS spectra as close to 90^o at all frequencies is preferred for obtaining high power densities and fast charging and discharging [2]. Electrochemical impedance spectroscopy was performed to estimate the ESR of the cell with different electrolytes and the Nyquist plots obtained for the SCs are as observed in Fig. 6(a).

The Nyquist plots for all the three cells demonstrate a semi-circle at the high frequency region and a straight line at the lower frequency region which is typical for symmetric carbon based SCs. The intercept of the plots with the real axis gives the equivalent series resistance (ESR) of the cell which can be used to obtain the maximum power or maximum power density that the SC can deliver [30]. The ESR values are related to the ionic conductivity of the cell which would imply that the SC with H_3PO_4 electrolyte should demonstrate the least ESR value. The ESR values obtained for H_2SO_4, H_3PO4 and Na_2SO_4 are 0.303 Ω, 0.388 Ω and 0.611 Ω respectively. It is observed that unlike the expected trend, SC with 0.5M H_2SO_4 electrolyte demonstrates the least ESR value which in agreement with the results obtained from the GCD studies. The results obtained vary from the expected trend which can be considered to be due to the vari-

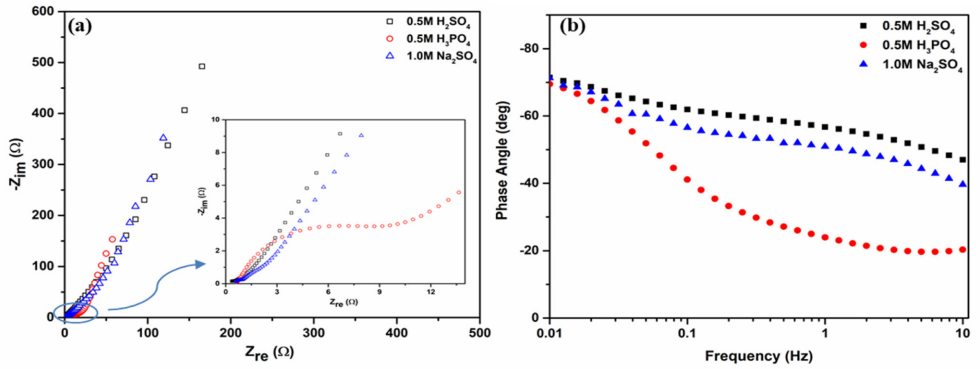

Fig. 6. (a) Nyquist plots up to end frequency of 10 mHz with magnification at the high frequency region (inset) and (b) Bode phase angle plots for cells with H_2SO_4, H_3PO_4 and Na_2SO_4

ation in the hydrated ion size and the accessibility to the interior of the nanostructure of rGO [28]. Apart from these, factors such as ionic adsorption, extent of ionization in solvent and ion pairing of solutes are known to affect the cell performance [2].

The results can be further validated using the Bode plots for the three electrolytes which is depicted in Fig. 6(b). An ideal SC with fast charge-discharge process exhibits a phase angle of close to -90°. The SC fabricated exhibits a phase angle approaching -72°, -71° and -69° for H_2SO_4, H_3PO4 and Na_2SO_4 respectively. The slight deviation from ideal phase angle of -90° can be attributed to the corrosive nature of the electrolyte for the acidic electrolytes [31] and to the low ionic mobility in case of neutral electrolyte. However, neutral electrolyte can be used for achieving higher energy density since they can be employed in larger working voltage of up to 1.6V and also provide a less corrosive environment [31-34].

4. Conclusions

In the present study, the performance of reduced graphene oxide based symmetric supercapacitors with different aqueous electrolytes. Wider operating voltage window for charging and discharging can be obtained if the aqueous electrolyte is replaced with an organic electrolyte based on acetonitrile or propylene carbonate. However, organic electrolytes pose a toxicity hazard are such SCs need to be fabricated in extremely controlled conditions. Also, cells based on organic electrolytes have lower power density as compared to their aqueous counterparts. Since such cells store energy due to pseudocapacitance or redox reactions occurring on the surface of the electrodes, the cycle life is lesser than the life obtained for their aqueous counterparts. The symmetric SC fabricated with H_3PO_4 electrolyte delivers the highest specific capacitance of 14 mF/cm^2 at a scan rate of 5 mV/s which is comparable to the values obtained from GCD studies where the SC delivered a specific capacitance of 11 mF/cm^2 at a current density of 0.16 mA/cm^2. However, the SC fabricated with H_2SO_4 electrolyte demonstrated the lowest ESR value of 0.303 Ω which implies that for fabricating an aqueous symmetric SC based on rGO as active material, H_3PO_4 electrolyte is more suited where high energy density is required where H_2SO_4 electrolyte for high power density applications.

Acknowledgement

The authors would like to thank the management of Central Power Research Institute, an autonomous institute under the Ministry of Power for their support in conducting the research work.

References

1. P. Simon, and Y. Gogotsi. 'Materials for electrochemical capacitors', *Nature Materials,* **7(11)**, 845-854 (2008).
2. B. E. Conway, '*Electrochemical supercapacitors: scientific fundamentals and technological applications*',

Springer Science & Business Media (2013).
3. W. Ma, S. Chen, S. Yang, W. Chen, W. Weng, Y. Cheng, and M. Zhu, 'Flexible all-solid-state asymmetric supercapacitor based on transition metal oxide nanorods/reduced graphene oxide hybrid fibers with high energy density', *Carbon*, **113**, 151-158 (2017).
4. Y. Liu, X. Miao, J. Fang, X. Zhang, S. Chen, W. Li, W. Feng, Y. Chen, W. Wang, and Y. Zhang, 'Layered-MnO_2 nanosheet grown on nitrogen-doped graphene template as a composite cathode for flexible solid-state asymmetric supercapacitor', *ACS Appl. Mater. Interfaces*, **8(8)**, 5251-5260 (2016).
5. X. Yang, H. Niu, H. Jiang, Q. Wang, and F. Qu, 'A high energy density all-solid-state asymmetric supercapacitor based on MoS_2/graphene nanosheets and MnO_2/graphene hybrid electrodes', *J. Mater. Chem. A*, **4(29)**, 11264-11275 (2016).
6. Wang, H. Zhang, and C. Cheng, 'Synthesis of hierarchical NiS microflowers for high performance asymmetric supercapacitor', *Chemical Engineering Journal*, **308**, 1165-1173 (2017).
7. J. Zhu, T. Feng, X. Du, J. Wang, J. Hu, and L. Wei, 'High performance asymmetric supercapacitor based on polypyrrole/graphene composite and its derived nitrogen-doped carbon nano-sheets', *Journal of Power Sources*, **346**, 120-127 (2017).
8. P. Bandyopadhyay, T. Kuila, J. Balamurugan, T. T. Nguyen, N. H. Kim, and J. H. Lee, 'Facile synthesis of novel sulfonated polyaniline functionalized graphene using m-aminobenzene sulfonic acid for asymmetric supercapacitor application', *Chemical Engineering Journal,* **308**, 1174-1184 (2017).
9. K. Rana, S. D. Kim, and J. H. Ahn, 'Additive-free thick graphene film as an anode material for flexible lithium-ion batteries' *Nanoscale*, **7**, 7065-7071 (2015).
10. M. Wang, L. D. Duong, N. T. Mai, S. Kim, Y. Kim, H. Seo, Y. C. Kim, W. Jang, Y. Lee, J. Suhr, and J. D. Nam, 'All-solid-state reduced graphene oxide supercapacitor with large volumetric capacitance and ultralong stability prepared by electrophoretic deposition method', *ACS Appl. Mater. Interfaces*, **7(2)**, 1348-1354 (2015).
11. H. Zanin, E. Saito, H. J. Ceragioli, V. Baranauskas, and E. J. Corat, 'Reduced graphene oxide and vertically aligned carbon nanotubes superhydrophilic films for supercapacitors devices', *Materials Research Bulletin,* **49**, 487-493 (2014).
12. J. L. Shi, W. C. Du, Y. X. Yin, Y. G. Guo, and L. J. Wan, 'Hydrothermal reduction of three-dimensional graphene oxide for binder-free flexible supercapacitors', *J. Mater. Chem. A*, **2(28)**, 10830-10834 (2014).
13. J. P. C. Trigueiro, R. L. Lavall, and G. G. Silva, 'Supercapacitors based on modified graphene electrodes with poly (ionic liquid)', *Journal of Power Sources*, **256**, 264-273 (2014).
14. D. Sun, X. Yan, J. Lang, and Q. Xue, 'High performance supercapacitor electrode based on graphene paper via flame-induced reduction of graphene oxide paper', *Journal of Power Sources*, **222**, 52-58 (2013).
15. T. Fan, W. Zeng, Q. Niu, S. Tong, K. Cai, Y. Liu, W. Huang, Y. Min, and A. J. Epstein, 'Fabrication of high-quality graphene oxide nanoscrolls and application in supercapacitor', *Nanoscale Res Lett*, **10(1)**, 192 (2015).
16. Z. Niu, L. Zhang, L. Liu, B. Zhu, H. Dong, and X. Chen, 'All-solid-state flexible ultrathin micro-supercapacitors based on graphene', *Advanced Materials*, **25(29)**, 4035-4042 (2013).
17. Y. Liang, Z. Wang, J. Huang, H. Cheng, F. Zhao, Y. Hu, L. Jiang, and L. Qu, 'Series of in-fiber graphene supercapacitors for flexible wearable devices', *J. Mater. Chem. A*, **3(6)**, 2547-2551 (2015).
18. D. Wang, Y. Min, Y. Yu, and B. Peng, 'A general approach for fabrication of nitrogen-doped graphene sheets and its application in supercapacitors', *Journal of colloid and interface science*, **417**, 270-277 (2014).
19. K. Gao, Z. Shao, X. Wu, X. Wang, Y. Zhang, W. Wang, and F. Wang, 'Paper-based transparent flexible thin film supercapacitors', *Nanoscale*, **5(12)**, 5307-5311 (2013).
20. F. T. Johra, and W. G. Jung, 'Hydrothermally reduced graphene oxide as a supercapacitor', *Applied Surface Science*, **357**, 1911-1914 (2015).
21. W. W. Liu, Y. Q. Feng, X. B. Yan, J. T. Chen, and Q. J. Xue, 'Superior micro-supercapacitors based on graphene quantum dots', *Advanced Functional Materials*, **23(33)**, 4111-4122 (2013).
22. A Daraghmeh, S. Hussain, I. Saadeddin, L. Servera, E. Xuriguera, A. Cornet, & A. Cirera, 'A study of carbon nanofibers and active carbon as symmetric supercapacitor in aqueous electrolyte: a comparative study', *Nanoscale Research Letters*, **12(1)**, 639 (2017).
23. R. Shao, J. Niu, J. Liang, M. Liu, Z. Zhang, M. Dou, Y. Huang, and F. Wang, 'Mesopore-and macropore-dominant nitrogen-doped hierarchically porous carbons for high-energy and ultrafast supercapacitors in non-aqueous electrolytes', *ACS applied materials & interfaces*, **9(49)**, 42797-42805 (2017).
24. B. Paulchamy, G. Arthi, and B. D. Lignesh, 'A Simple Approach to Stepwise Synthesis of Graphene Oxide Nanomaterial', *J Nanomed Nanotechnol*, **6(1)**, 253 (2015).
25. D. C. Marcano, D. V. Kosynkin, J. M. Berlin, A. Sinitskii, Z. Sun, A. Slesarev, L. B. Alemany, W. Lu, and J. M. Tour, 'Improved synthesis of graphene oxide', *ACS nano*, **4(8)**, 4806-4814 (2010).
26. S. Park, J. An, J. R. Potts, A. Velamakanni, S. Murali, and R. S. Ruoff, 'Hydrazine-reduction of graphite-and graphene oxide', *Carbon*, **49(9)**, 3019-3023 (2011).
27. Z. S. Wu, K. Parvez, X. Feng, and K. Müllen, 'Graphene-based in-plane micro-supercapacitors with high power and energy densities', *Nature communications*, **4(1)**, 1-8 (2013).
28. A. Bello, F. Barzegar, M. J. Madito, D. Y. Momodu, A. A. Khaleed, T. M. Masikhwa, J. K. Dangbegnon, and N.

Manyala, 'Electrochemical performance of polypyrrole derived porous activated carbon-based symmetric supercapacitors in various electrolytes', *RSC advances*, **6(72)**, 68141-68149 (2017).
29. C. Zhong, Y. Deng, W. Hu, J. Qiao, L. Zhang, and J. Zhang, 'A review of electrolyte materials and compositions for electrochemical supercapacitors', *Chem. Soc. Rev.*, **44(21)**, 7484-7539 (2015).
30. C. X. Guo, and C. M. Li, 'A self-assembled hierarchical nanostructure comprising carbon spheres and graphene nanosheets for enhanced supercapacitor performance', *Energy Environ. Sci.*, **4(11)**, 4504-4507 (2011).
31. Q. Abbas, D. Pajak, E. Frąckowiak, and F. Béguin, 'Effect of binder on the performance of carbon/carbon symmetric capacitors in salt aqueous electrolyte', *Electrochimica Acta*, **140**, 132-138 (2014).
32. R. Shao, J. Niu, J. Liang, M. Liu, Z. Zhang, M. Dou, Y. Huang, and F. Wang, 'Mesopore-and macropore-dominant nitrogen-doped hierarchically porous carbons for high-energy and ultrafast supercapacitors in non-aqueous electrolytes', *ACS Appl. Mater. Interfaces*, **9(49)**, 42797-42805 (2017).
33. S. Sathyamoorthi, S. Tubtimkuna, and M. Sawangphruk, 'Influence of structures and functional groups of carbon on working potentials of supercapacitors in neutral aqueous electrolyte: In situ differential electrochemical mass spectrometry', *Journal of Energy Storage*, **29**, 101379, (2020).
34. Kuldeep Rana; K. Naga Mahesh; J. H. Ahn; Vinay Pratap Singh, 'Synthesis of additive free electrode material of supercapacitor for energy storage applications' pp.448, *11th International Conference on Industrial and Information Systems (ICIIS)*, (2016).